Chinese Journal of Aeronautics, (2019), 32(9): 2095–2108

Chinese Society of Aeronautics and Astronautics
& Beihang University

Chinese Journal of Aeronautics

cja@buaa.edu.cn
www.sciencedirect.com

Six sigma robust design optimization for thermal protection system of hypersonic vehicles based on successive response surface method

Jingjing ZHU [a], Xiaojun WANG [a,*], Haiguo ZHANG [b], Yuwen LI [b], Ruixing WANG [c], Zhiping QIU [a]

[a] *Institute of Solid Mechanics, School of Aeronautic Science and Engineering, Beihang University, Beijing 100083, China*
[b] *The 704 Research Institute of CSIC, Shanghai 200031, China*
[c] *Institute of Mechanics, Chinese Academy of Science, Beijing 100190, China*

Received 18 July 2018; revised 8 October 2018; accepted 3 January 2019
Available online 30 May 2019

KEYWORDS

Hypersonic vehicle;
Six sigma robust optimization;
Successive response surface;
Thermal protection system;
Uncertainty

Abstract Lightweight design is important for the Thermal Protection System (TPS) of hypersonic vehicles in that it protects the inner structure from severe heating environment. However, due to the existence of uncertainties in material properties and geometry, it is imperative to incorporate uncertainty analysis into the design optimization to obtain reliable results. In this paper, a six sigma robust design optimization based on Successive Response Surface Method (SRSM) is established for the TPS to improve the reliability and robustness with considering the uncertainties. The uncertain parameters related to material properties and thicknesses of insulation layers are considered and characterized by random variables following normal distributions. By employing SRSM, the values of objective function and constraints are approximated by the response surfaces to reduce computational cost. The optimization is an iterative process with response surfaces updating to find the true optimal solution. The optimization of the nose cone of hypersonic vehicle cabin is provided as an example to illustrate the feasibility and effectiveness of the proposed method.

1. Introduction

The Reusable Hypersonic Vehicle (RHV) is a fully reusable transportation system that operates at hypersonic speed ($Ma > 5$) for a significant part of its trajectory. During reentry into the atmosphere at hypersonic speed, one of the main challenges is that the RHV is subjected to severe aerodynamic heating upon the surfaces which are exposed to the surroundings, especially, the harshest heating environments locate on

* Corresponding author.
E-mail address: xjwang@buaa.edu.cn (X. WANG).
Peer review under responsibility of Editorial Committee of CJA.

Production and hosting by Elsevier

https://doi.org/10.1016/j.cja.2019.04.009

the nose of the vehicle and the wing leading edges due to the stagnation point heating. In order to successfully achieve hypersonic flight, a Thermal Protection System (TPS) is designed to protect the inner structures of hypersonic vehicles from extreme temperature. The research into thermal protection technology is ongoing and becomes a hot issue.[1–3]

In order to make hypersonic vehicles more durable, operable and cost effective, the current design of TPS is mainly carried out to realize the minimum weight and better insulation performance by defining the material, arrangement and thickness.[4–6] For instance, Garcia and Fowler[7] used a first-order optimization algorithm to minimize the weight of the TPS for reentry space shuttle. Shi et al.[8] investigated the optimization design of TPS formulated with mass per unit area of the TPS as the objective function considering the relationships of multi-discipline in the TPS. Xie et al.[9] investigated the weight optimization for a corrugated sandwich panel which served as an Integrated Thermal Protected System (ITPS). Normally, these existing studies were carried out under the assumption that all of the parameters involved in the heat transfer analysis were deterministic. However, due to the materials dispersion, manufacturing process constraints and operating condition deterioration of production stages, the presence of uncertainty in material properties and geometry is intrinsic and it markedly affects the temperature response of TPS. The uncertainty of temperature response is significant to the design of TPS in which even a few degrees of temperature variability may cause serious consequences.[10] Sachin and Mahulikar[11] pointed out that there were physical complexities and uncertainties associated with the analytical models which were used for TPS performance. It is critical to consider these variations during the optimization, in order to ensure the safety of the final design and the performance constraints even in the presence of uncertainty. Wright[12] and Ravishankar et al.[13] proposed the uncertainty analysis approaches by using Monte Carlo method for probabilistic sensitivity and uncertainty propagation analysis of TPS material responses. Therefore, it is requisite to include uncertain analysis into the design optimization for TPS.

Traditional deterministic optimization considers the uncertainties through the use of empirical safety factors based on experience. This practice often leads to over-designed products. It cannot provide insights into the actual margin of safety of a design, and the effects of individual uncertainties cannot be distinguished either. Therefore, uncertainty-based design methods, which combine optimization approaches with uncertain analysis,[14–17] have been developed in recent years. The uncertainty-based design generally includes structural reliability design,[18,19] robust design,[20,21] etc. The structural reliability design converts the deterministic constraints into reliability constraints by reliability analysis. The reliability analysis evaluates the probability of failure or reliability index of the design with respect to specific structural performance constraints. The uncertainty-based analysis and optimization design for TPS is promising, yet insufficient up to now. Some researchers have made a few attempts in this field. Kolodziej and Rasky[22] used the non-dimensional load interference method for estimating thermal reliability from an assessment of TPS uncertainties. Kumar et al.[23] investigated the probabilistic optimization of ITPS that combines the thermal protection function with the structural load carrying function. Antonio and Marchetti[24] presented a statistical methodology based on the Monte Carlo method to perform a size optimization of an ablative thermal protection system for atmospheric entry vehicles. However, the objective of the reliability-based optimization is evaluated at the mean value point. The design only accounts for the shift of the mean values of responses from constraint boundaries, but not considers the size of the response distributions and the possibility of reducing the variation of response.

Recently, the six sigma robust optimization has been widely applied to quality engineering.[25–27] Six sigma robust optimization is an advanced design method combining six sigma quality management theory and robust optimization, which aims to minimize the objective and satisfy the reliability design requirements. The six sigma robust optimization considers both the optimality and robustness of the objective to achieve lower sensitivity of objective performance to the uncertainties. Many scholars have carried out a lot of studies in this field. Roger et al.[28] proposed a conceptual definition and underlying theory of six sigma based on the grounded theory and previous literature available. Patrick et al.[29] presented a six sigma based probabilistic design optimization formulation that combined the structural reliability and robust design with six sigma philosophy. He pointed out that design quality came at a cost and the tradeoff between the optimization objective and the reliability (or sigma level) should be considered in the design. On the basis of the "Design For Six Sigma" (DFSS), a new method "Design For Multi-Objective Six Sigma (DFMOSS)" that combined the theory of DFSS and Multi-Objective Evolutionary Algorithm (MOEA) was presented.[30,31] In order to improve both the reliability and robustness of the design, this paper proposes a six sigma robust optimization model to carry out a probabilistic optimization for the TPS of hypersonic vehicles.

In the transient heat transfer analysis for TPS along the entire trajectory, the Finite Element (FE) analysis needs to be continued for long time to capture the peak temperature, which seriously reduces the efficiency of optimization. Since the optimization process for TPS needs plenty of repeated individual FE simulations, the computation may be extremely expensive for broad design space. Moreover, probabilistic analysis and reliability-based optimization will further increase the computation cost and the fact that TPS components are generally made of composite materials further increases the uncertainties in material properties.[13] To reduce the computational cost, many approximation models were put forward to generate surrogates of the FE simulations. The sampling data are chosen by Design of Experiment (DOE) and the surrogate models can be utilized for optimizations as substitutes of FE simulations. There are many types of surrogate models, such as Kriging model,[32] Neural Networks model,[33] Response Surface Approximation (RSA),[34–37] etc. As the form of an approximate function is assumed first, the Response Surface Method (RSM) often serves as an effective statistical method. It uses fewer resources and quantitative data to solve a multivariate optimization problem. Theodore et al.[38] utilized RSM to achieve the deterministic and reliability optimizations for the integrated cryogenic propellant tank of a reusable launch vehicle. Ravishankar et al.[13] studied the uncertainty characterization and predicted the probability of failure for an ITPS by using RSAs. The accuracy of response surface approximation has a great influence on the optimal solution. In some cases, though the quality of the approximation is acceptable across the entire design space, the error near the design point may be high resulting in a poor optimum design. In the past

decades, many methods have been actively studied to improve the accuracy and computational efficiency of RSM for optimization problem, one of which is the Successive Response Surface Method (SRSM).[39] Generally, the smaller the design space is, the greater the accuracy of approximation will be. In addition, the researchers have developed other methods that can iteratively improve the accuracy of the response surface modeling. Kim and Na[40] proposed an improved sequential response surface method to evaluate the reliability inherent in nonlinear functions. Giunta et al.[41] utilized the variable-complexity response surface modeling method to reduce the design space for the region of interest, which has been widely used in structural designs. Wang[42] presented an improved Adaptive Response Surface Method (ARSM) with global convergence and high optimization efficiency for high-dimensional design problems. Therefore, this paper employs the successive response surface method during the six sigma robust optimization process to improve the accuracy of response surface, which is rare in the field of TPS optimization considering uncertainties to the author's knowledge.

In this paper, an efficient and effective optimization approach obtained by coupling six sigma design, TPS thermal analysis and SRSM is proposed to carry out a probabilistic optimization for the TPS of hypersonic vehicles. The TPS model used in this paper is a typical structural component of the hypersonic vehicle. The presented method will provide more reliable and robust design for the TPS while considering the effects of uncertainties on the structural responses, and the computation cost will be reduced significantly. The remainder of this paper is organized as follows. Section 2 describes the configuration of the TPS model of a typical hypersonic vehicle and the governing equations of heat transfer analysis. The deterministic optimization model and six sigma robust optimization model for the TPS are established in Section 3. In Section 4, the optimization approach based on SRSM is presented and the complete strategy procedure of this paper is elaborated. In Section 5, a model of the nose cone of a hypersonic vehicle cabin is used to illustrate the application of the proposed methodology. Finally, some conclusions are summarized in Section 6.

2. Configuration and governing equations of TPS

2.1. Description of TPS configuration

The TPS is attached to the outer surface of the hypersonic vehicle structure, such as the vehicle cabin as depicted in Fig. 1. The TPS modeled in this paper consists of three layers, i.e. an external panel and two insulation layers, which are bonded together with adhesive. The external panel serves as a heat shield, which insulates the insulation layers from external ambient to protect the insulation layers from the damage due to high temperature and aerodynamic pressure. The material used for the first layer should be capable of withstanding high temperature and the second layer is filled with the material that has prominent insulation capacity at the relatively lower service temperature.[43] Generally, the thickness of the external panel is much smaller than those of insulation layers.

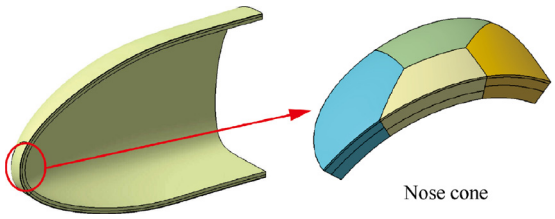

Fig. 2 Multi-blocks structure of TPS.

In practical engineering, the TPS generally adopts the multi-blocks structure (see Fig. 2), namely the whole TPS is divided into several blocks, one of which is connected to another by fastener, and the gap is filled with sealing materials. Actually, the thicknesses of the insulation layers of different blocks can be inconsistent with each other due to the complex thermal environment.

2.2. Transient heat transfer analysis for TPS

The loads and thermal boundary conditions imposed on the outer surface of TPS are shown in Fig. 3. A large portion of heat is radiated out to the ambient by the outer surface. The inner surface of the second insulation layer is assumed to be perfectly insulated. That is to say, the heat convection between the TPS and the interior of vehicle is not considered. With this

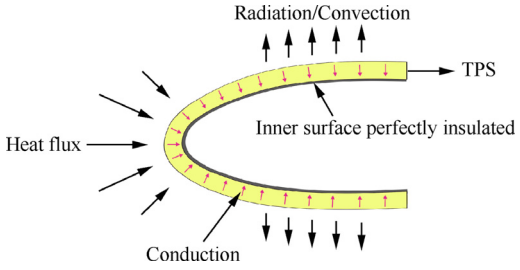

Fig. 3 Loads and thermal boundary conditions imposed on the outer surface of TPS.

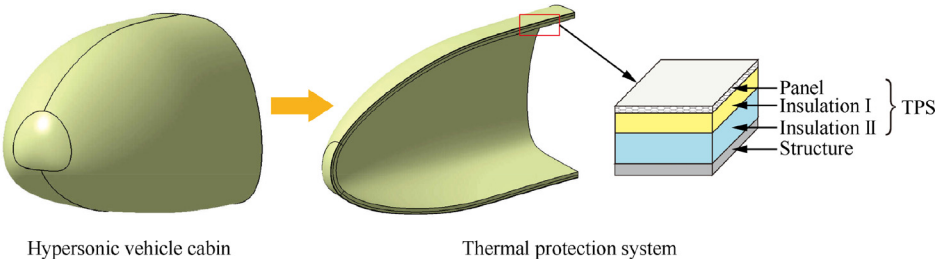

Fig. 1 Depiction of TPS configuration of a hypersonic vehicle.

assumption, the optimization would lead to a conservative design. Radiation and convection through the insulation material are ignored and only the conduction is taken into consideration. The initial temperature of the whole model is assumed to be a constant at the start of reentry. Besides the above assumptions, the effect of the adhesive on heat transfer is ignored and the interfaces between adjacent layers of TPS are assumed to be perfectly conductive, which indicates that there exists no thermal contact resistance. Furthermore, since the gap between two blocks is filled with insulation materials with low thermal conductivity, the interfaces of different blocks are assumed to be adiabatic.

The basic governing equation of heat conduction can be described by the following partial differential form

$$\frac{\partial T}{\partial t}=\frac{k}{\rho c}\left(\frac{\partial^2 T}{\partial x^2}+\frac{\partial^2 T}{\partial y^2}+\frac{\partial^2 T}{\partial z^2}\right) \tag{1}$$

where T is the temperature, t is the time, K, ρ, c denote the thermal conductivity, density, and specific heat, respectively, x, y and z denote the coordinates along x-, y- and z-axes, respectively.

The initial condition for the thermal analysis is

$$T|_{t=0}=T_0 \tag{2}$$

where T_0 is the initial temperature and assumed to be 300 K in this paper.

The incident heat flux entering the TPS can be expressed as

$$q_{\text{in}}=-k\left.\frac{\partial T}{\partial n}\right|_s \tag{3}$$

where q_{in} is the incident heat flux, n denotes the normal direction of the outer surface s.

The radiation to ambient is determined by

$$q_{\text{r}}=\varepsilon\sigma\left(T_{\text{s}}^4-T_{\text{a}}^4\right) \tag{4}$$

where q_{r} stands for the radiation heat flux, ε is the surface emissivity of the outer surface which typically has a value of 0.8–0.85,[44] σ is Stefan-Boltzmann constant, T_{s} denotes the temperature of outer surface and T_{a} denotes the ambient temperature.

Based on the surface energy balance condition, the boundary imposed on the outer surface yields

$$q_{\text{w}}=q_{\text{in}}+q_{\text{r}} \tag{5}$$

where q_{w} is the heat flux load caused by aerodynamic heating.

After aircraft touchdown, a natural convection to the ambient is used as the boundary condition imposed on the outer surface (see Fig. 3)

$$q_{\text{c}}=\alpha(T_{\text{s}}-T_{\text{a}}) \tag{6}$$

where q_{c} represents the convection heat flux, α is the convection coefficient.

3. Deterministic and six sigma robust design optimization for TPS

3.1. Deterministic optimization for TPS

The TPS will not only fulfill the required thermal protection functions, but also must be as lightweight as possible to minimize operational costs. In this section, an optimization model is defined to determine the optimal thicknesses of insulation layers aiming at minimizing the total weight while maintaining the structures with acceptable temperature limits. The design variables for the optimization are the thicknesses of insulation layers of the TPS, which can be denoted by a vector $\boldsymbol{d}$. Two critical constraints are considered for the optimization to guarantee the functions of TPS and underlying structures: (A) the maximum temperature of each insulation layer must be less than the service temperature limit of the insulation material and (B) the maximum temperature of the inner surface of TPS must be less than the critical temperature that is safe for the underlying structure/screw compartment of the vehicle. The optimization problem of the TPS can be described mathematically as follows:

$$\begin{cases}\text{find} & \boldsymbol{d}\\ \min & W(\boldsymbol{d})\\ \text{s.t.} & T_{1,\max}(\boldsymbol{d})\le T_1^{\text{limit}}\\ & T_{2,\max}(\boldsymbol{d})\le T_2^{\text{limit}}\\ & T_{\text{inner},\max}(\boldsymbol{d})\le T_{\text{inner}}^{\text{limit}}\\ & \boldsymbol{d}^{\text{L}}\le\boldsymbol{d}\le\boldsymbol{d}^{\text{U}}\end{cases} \tag{7}$$

where $\boldsymbol{d}=[d_1\ d_2\cdots d_n]^{\text{T}}$ is the vector of design variables, $W(\boldsymbol{d})$ represents the weight of TPS, $T_{1,\max}$, $T_{2,\max}$, and $T_{\text{inner},\max}$ are the maximum temperatures of the first insulation layer, second insulation layer and inner surface, respectively, T_1^{limit}, T_2^{limit}, and $T_{\text{inner}}^{\text{limit}}$ are the temperature limits of the first insulation layer, second insulation layer and inner surface, respectively, $[\boldsymbol{d}^{\text{L}},\boldsymbol{d}^{\text{U}}]$ is the range of the vector of design variables.

3.2. Six sigma robust design optimization for TPS

In practice, the solution obtained by deterministic optimization is often close to the critical constraints, which will result in an unreliable design due to the fluctuation existing in input parameters or environment. Reliability-based optimization focuses on the effects of random design variables, in which the optimal solution is shifted away from constraint boundaries to improve design reliability. To shrink the performance variation, robust design is implemented to decrease the sensitivity of design response to uncertainties. By combining reliability-based optimization, robust design and six sigma philosophy, Design For Six Sigma (DFSS)[29,30,45] is proposed to improve design quality, as illustrated in Fig. 4. In "shift", the performance distribution is shifted until an acceptable level of reliability (area of distribution inside constraint) is achieved. In "shrink", the performance variation is shrunk to reduce the potential performance loss associated with the tails of the distribution and thus reduce the sensitivity and improve the robustness. In "shift + shrink", with both shift and shrink, the reliability level is achieved and the robustness is improved.

The one consistency between the measures of reliability and robustness is the measure of variation: sigma. The performance variation can be characterized as "sigma level n", as illustrated in Fig. 5. The areas under the normal distribution associated with each σ-level relate directly to the reliability (e.g. $\pm1\sigma$ is equivalent to a reliability of 68.26%). Larger σ-level indicates smaller variation, i.e. more robust characteristic. The DFSS is proposed to achieve 6σ quality, which is defined

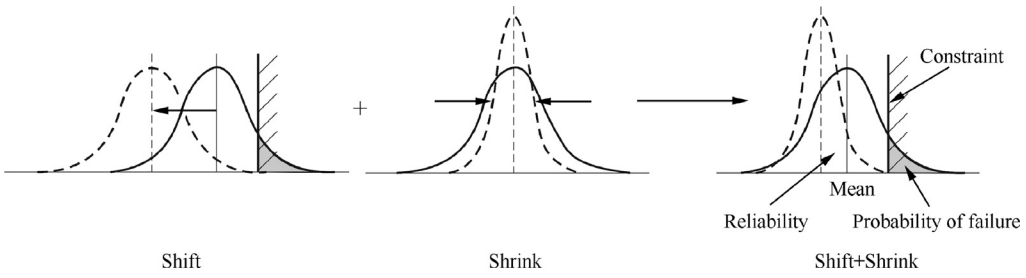

Fig. 4 Improvement of reliability and robustness.

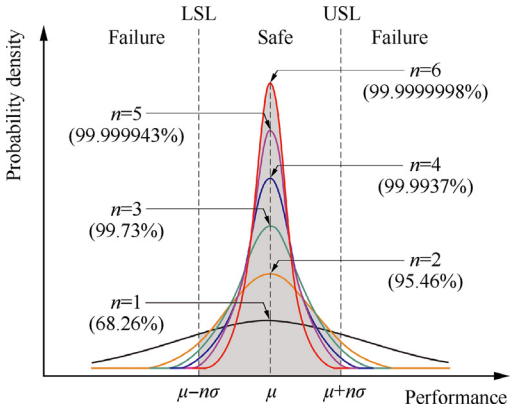

Fig. 5 Characteristic of sigma level n (LSL: lower specification limit, USL: upper specification limit).

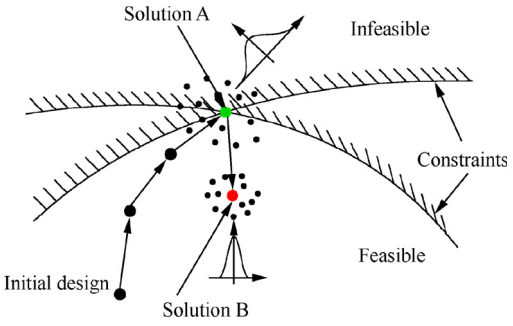

Fig. 6 Principle of six sigma robust design.

to maintain six sigma ($\mu \pm 6\sigma$) performance variation within the specification limits.

To improve the reliability and robustness, the deterministic optimization for TPS is converted to a six sigma robust design optimization by considering the uncertainties related to the geometric parameters and material properties. The six sigma robust optimization is established to minimize the mean and variation of performance response with constraints imposed on the input variables and output responses. The input constraints are random design variable bounds and the output constraints can be reliability or sigma level quality striving to maintain performance variation within the defined acceptable limits. The formulation can be expressed as follows:

$$\begin{cases} \text{find} & \boldsymbol{d} \\ \min & \lambda_1 \mu_W^2 + \lambda_2 \sigma_W^2 \\ \text{s.t.} & \mu_{T_{1,\max}} + 6\sigma_{T_{1,\max}} \le T_1^{\text{limit}} \\ & \mu_{T_{2,\max}} + 6\sigma_{T_{2,\max}} \le T_2^{\text{limit}} \\ & \mu_{T_{\text{inner},\max}} + 6\sigma_{T_{\text{inner},\max}} \le T_{\text{inner}}^{\text{limit}} \\ & \boldsymbol{d}^{\text{L}} + 6\sigma_{\boldsymbol{d}} \le \mu_{\boldsymbol{d}} \le \boldsymbol{d}^{\text{U}} - 6\sigma_{\boldsymbol{d}} \end{cases} \tag{8}$$

where μ and σ denote the mean value and standard variation of structural weight or temperature constraint which are functions of the design variables and random input variables, λ_1 and λ_2 are the weight coefficients for the mean and standard variation of structural weight, $\boldsymbol{d}^{\text{L}}$ and $\boldsymbol{d}^{\text{U}}$ are the lower limit and upper limit of design variable vector, respectively. The principle of six sigma robust optimization is illustrated in Fig. 6 which shows that the solution B obtained by six sigma robust optimization has higher reliability and robustness as a comparison with the solution A obtained by deterministic optimization.

4. Successive response surface method based design optimization

In this paper, the vehicle is subjected to time varying aerodynamic heating load in the course of flight trajectory. As shown in Fig. 7, the TPS was heated up by the heat flux load before t_0 in the trajectory. After t_0, the aerodynamic heating ends but the temperature of TPS will continue to rise due to the heat transfer along the thickness direction. Consequently, the thermal analysis of TPS needs to be continued for long time to capture the peak temperature. For the probabilistic analysis and optimization with considering the uncertainties, it would require numerous simulations to study the uncertain propagation which may be extremely expensive for broad design space. In addition, the complexity of the solid model of the TPS of hypersonic vehicles will also lead to high computational expense. Therefore, the computation cost will be unbearable if the analysis was carried out by FE simulation.

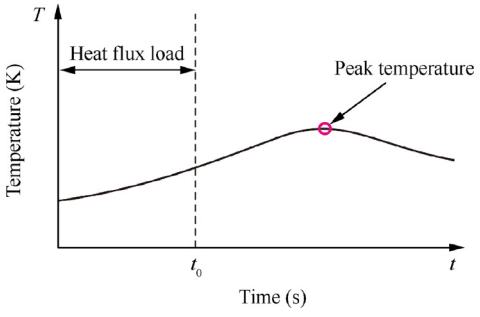

Fig. 7 Temperature profile of TPS with time.

4.1. Construction of response surface approximation

In this work, quadratic RSAs are used to construct the objective and constraints as functions of input parameters, since it is simple, easy to implement and has reasonable accuracy for concept and preliminary design of structure.[5] During optimization process, the quadratic response surfaces of objective function and constraints are constructed as follows:

$$\tilde{y} = \beta_0 + \sum_{i=1}^{M} \beta_i x_i + \sum_{i=1}^{M} \beta_{ii} x_i^2 + \sum_{i=1}^{M} \sum_{j=1}^{M} \beta_{ij} x_i x_j \tag{9}$$

where $\tilde{y}$ is the approximation of output response including the objective function W or temperature constraints $T_{1,\max}, T_{2,\max}, T_{\text{inner},\max}, \beta$, represents the unknown coefficient, $\boldsymbol{X} = [x_1 \ x_2 \cdots x_M]$ represents the input parameter vector which may be design variables, random variables or both, and M is the total number of input parameters.

Before constructing the RSA, a DOE should be implemented to locate the sampling points in the design space. In this paper, the Optimal Latin Hypercube (OLH) is chosen for DOE because of its low computational cost and uniformity of samples resulting in better approximations.[46]

4.2. Successive response surface method

In the optimization procedure, the estimations of output responses are implemented by RSM. Generally, the quality of the approximation is evaluated by separate data set or cross-variation to ensure that the approximation has an acceptable average error across the entire design space. However, the error near the design point may be high resulting in a poor optimum design. Therefore, the response surface updating is needed in the optimization process to obtain a design with a higher probability of success.

In order to ensure the solution converge to the true optimum, the accuracy of RSA is improved by reconstruction via adding additional sampling points from the new subregion centered around the optimal solution into the previous sampling data set. The subregion is updated by shift and reduction from the previous one, as shown in Fig. 8. Moreover, the optimal point serves as a starting point for the next iteration during optimization procedure. The bounds of the i-th design variable for the $k+1$-th subregion can be determined by

$$\begin{aligned} d_{i,k+1}^{\mathrm{L}} &= d_{i,k}^{*} - \tfrac{1}{2}\lambda_{k+1}\left(d_{i,k}^{\mathrm{U}} - d_{i,k}^{\mathrm{L}}\right) \\ d_{i,k+1}^{\mathrm{U}} &= d_{i,k}^{*} + \tfrac{1}{2}\lambda_{k+1}\left(d_{i,k}^{\mathrm{U}} - d_{i,k}^{\mathrm{L}}\right) \end{aligned} \tag{10}$$

where $d_{i,k}^{\mathrm{L}}$ and $d_{i,k}^{\mathrm{U}}$ are the lower and upper bounds of the i-th design variable for the k-th subregion, respectively, $d_{i,k+1}^{\mathrm{L}}$ and $d_{i,k+1}^{\mathrm{U}}$ are the lower and upper bounds of the i-th design variable for the $k+1$-th subregion, respectively, $d_{i,k}^{*}$ is the optimal point in the k-th iteration, and λ_{k+1} is the fraction parameter which can be calculated by

$$\lambda_{k+1} = \max_{1 \le i \le n} \lambda_i^{k+1} \tag{11}$$

where λ_i^{k+1} is the fraction parameter for the i-th design variable which can be obtained by

$$\lambda_i^{k+1} = \eta + (\gamma - \eta) \frac{\left| d_{i,k}^{*} - \frac{d_{i,k}^{\mathrm{L}} + d_{i,k}^{\mathrm{U}}}{2} \right|}{\frac{d_{i,k}^{\mathrm{U}} - d_{i,k}^{\mathrm{L}}}{2}} \tag{12}$$

where $\eta = 0.5$ and $\gamma = 1.0$ for quadratic approximations[39] in this study. In addition, γ are chosen as $\gamma = 0.8$ for linear approximations in order to counter the cycling effect as commonly encountered when using successive linear approximations.

The convergence criterion used in this research is the relative change in the approximate objective values in the last two iterations which can be expressed by

$$\left| \frac{G(\boldsymbol{d}_{k+1}) - G(\boldsymbol{d}_k)}{G(\boldsymbol{d}_k)} \right| < \varepsilon \tag{13}$$

where ε is the convergence control parameter and its value is considered as 0.001, $G(\boldsymbol{d}_k)$ and $G(\boldsymbol{d}_{k+1})$ denote the approximations of the objective for the k-th and $k+1$-th iterations, respectively.

Fig. 9 illustrates the optimization process based on SRSM and the detailed computational procedure can be summarized as follows:

Step 1. The first RSA denoted by $\tilde{y}_1$ is established by DOE for the initial design space. Then the RSA is used to obtain the optimal point $\boldsymbol{d}_1$ by optimization procedure. From Fig. 9, it can be seen that there is a relatively large deviation between $\tilde{y}_1$ and the actual response y around $\boldsymbol{d}_1$. Therefore, the accuracy of RSA around $\boldsymbol{d}_1$ needs to be improved to obtain the actual optimal solution.

Step 2. The optimal point $\boldsymbol{d}_1$ is used as the new center point to construct a subregion, in which M additional sampling points are created and added into the previous sampling data set.

Step 3. A new RSA $\tilde{y}_2$ will be constructed by using the new sampling data set and the optimization is repeated to obtain the optimal point $\boldsymbol{d}_2$.

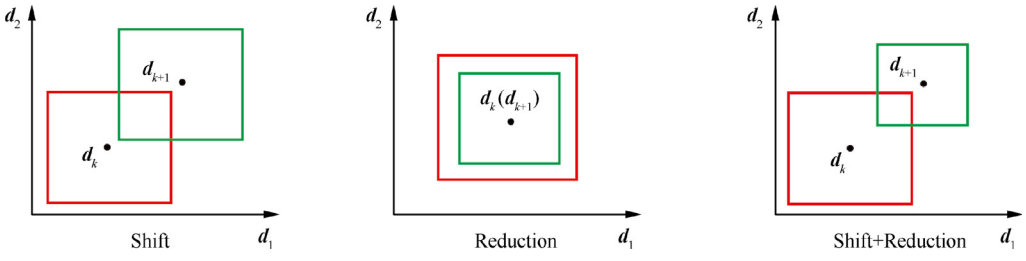

Fig. 8 Updating of subregion for RSA reconstruction.

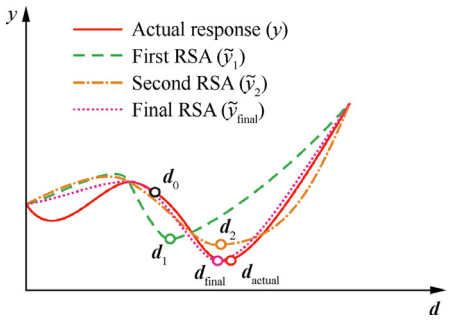

Fig. 9 Optimization process based on SRSM.

Step 4. By the same way, the processes of RSA reconstruction and optimization are repeated until the convergence condition is satisfied and the final approximate optimal solution $\boldsymbol{d}_{\text{final}}$ that is very close to the actual solution $\boldsymbol{d}_{\text{actual}}$ can be obtained.

4.3. Strategy procedure

In this subsection, we will elaborate the design procedure of the deterministic optimization and six sigma robust optimization for the TPS of hypersonic vehicles as follows:

Step 1. *Initialize design variables*. The geometric parameters are selected as the design variables for this optimization and their nominal values are defined as the initial values.

Step 2. *Create RSA*. To reduce the computation cost, the RSAs are created to evaluate the output responses, including objective function and constraints. The sampling points of input parameters, including design variables and random parameters, are generated by using OLH.

Step 3. *Construct and solve deterministic optimization problem*. Construct the deterministic optimization and the model can be mathematically written as Eq. (7). The overall weight of TPS is set as the objective function to be minimized and the critical temperatures of insulation layers and inner surface are considered as the constraints that maintain the functions of TPS and underlying structure of vehicle.

Step 4. *Update RSA*. The RSA will be updated in the optimization process to improve the analysis precision. The optimal solution is employed as the sampling center to construct additional sampling points, which is used to create a new RSA along with existing sampling points. If the relative change in the approximate objective values in the last two iterations is less than ε, turn to Step 5, otherwise, turn back to Step 3 to repeat the optimization process.

Step 5. *Perform quality analysis*. To analyze the quality of design, the quality of the deterministic optimum solution is measured by six sigma analysis to obtain the reliability or sigma level of the design.

Step 6. *Establish six sigma robust optimization model*. To improve the quality of design, the deterministic optimization is converted into a six sigma robust optimization formulated as Eq.(8). The objective is to improve the robustness by minimizing both mean value and standard variation of the performance response. The constraints are reformulated as quality constraints which satisfy six sigma level. The six sigma robust optimization starts with the deterministic optimal solution.

Step 7. *Update RSA*. After the initial optimal solution is obtained, the RSA will be updated by the same way used in Step 4.

Step 8. *Obtain optimal solution*. Conduct Step 6 to Step 7 until the convergence condition is satisfied and the optimal solution can be obtained.

The flowchart of the optimization procedure is shown in Fig. 10.

5. Demonstrative example

5.1. Thermal analysis

The nose cone of a typical hypersonic vehicle cabin (see Fig. 2) is selected as the application to demonstrate the effectiveness of the proposed optimization strategy. Since the thickness of external panel is much smaller than that of insulation layer, it is not chosen as the design variable and is held at a constant value of 5 mm. For simplicity, the thicknesses of the first or second insulation layer of all blocks are assumed to be the same. Therefore, the geometric parameters to be optimized include: the thickness of first insulation layer h_1 and the thickness of second insulation layer h_2 with initial values of 22 mm and 32 mm, respectively. The material properties of the panel and insulation layers, including thermal conductivity k, specific heat c, density ρ, are listed in Table 1.

To properly represent the heating trend along the entire trajectory, 55 points are selected from the trajectory and the time interval between adjacent points is 20 s. The heat flux imposed on the TPS and ambient temperature are schematically illustrated in Fig. 11, which are obtained from a real flight test. As shown in Fig. 11, the incident heat flux load is imposed on the outer surface before 1100 s (reentry phase) and there is no heat input after 1100 s (landing phase). As discussed in Section 2, the outer surface of TPS has radiation boundary condition during reentry and convective heat loss is also applied after landing. The radiation is determined by the emissivity ε of the outer surface with a value of 0.85 and the convection coefficient α is assumed to be $6.5\text{W}/(\text{m}^2 \cdot \text{K})$.[43] The maximum temperature responses of the external panel and insulation layers are calculated by commercial software ANSYS and the finite element model is shown in Fig. 12. Due to the symmetry of the structure, thermal loads and boundaries, only half the model is built for calculation.

After landing, the transient heat transfer analysis continues another 5400 s to capture the peak temperatures. The detailed results are depicted in Fig. 13, which illustrates the maximum temperature profiles of external panel, insulation layers and inner surface with time. It shows that the temperatures of external panel, insulation layers and inner surface increase because of aerodynamic heating during reentry process. The external panel reaches its peak temperature rapidly at about 620 s with a value of 1752.77 K and the maximum temperature of the first insulation layer reaches at 620 s with the same value as well. After 1100 s, there is no heat flux loading anymore, but the inner surface will continue to be heated up caused by the heat transfer along the thickness direction. The peak temperature $T_{\text{inner,max}}$ is reached at about 5800 s with a value of 411.72 K and then begins to decrease slowly.

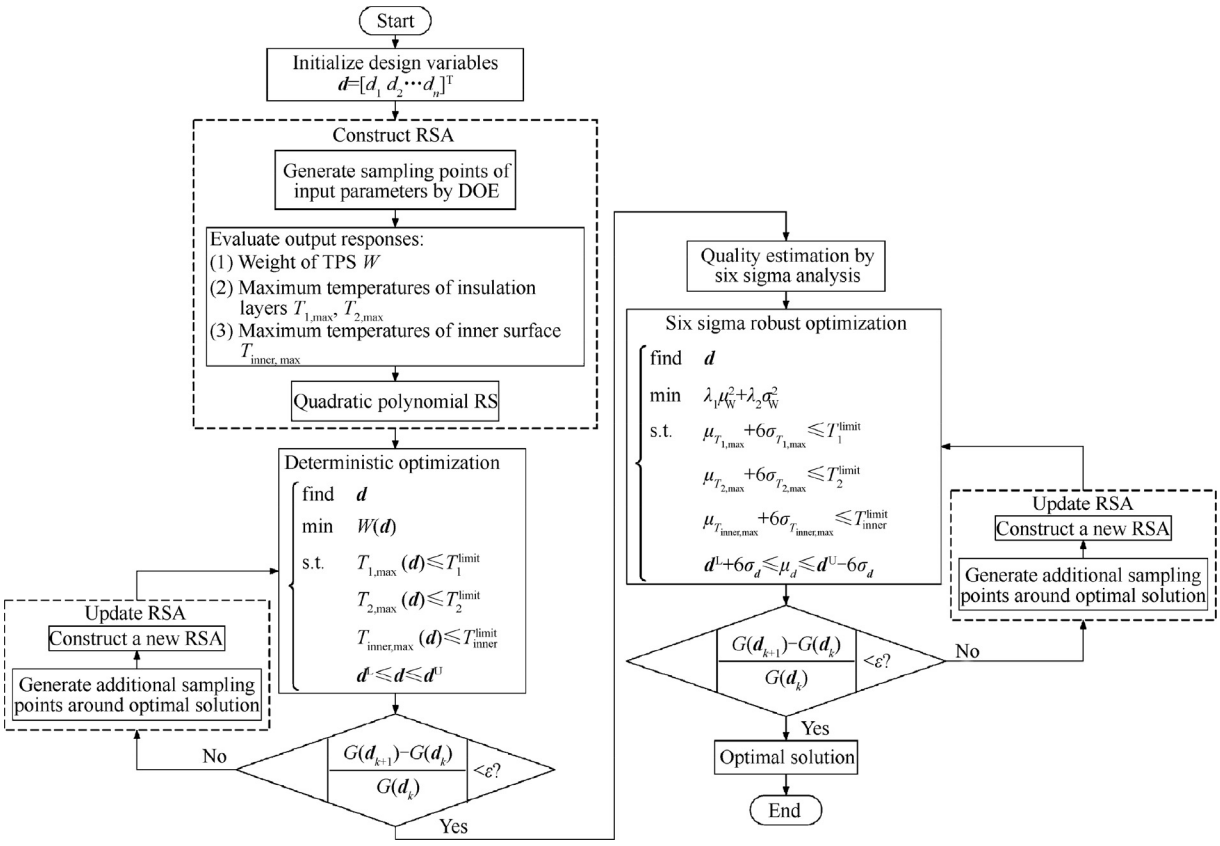

Fig. 10 Flowchart of the optimization procedure.

Table 1 Material properties of panel and insulation layers.

Material	$k\left(\mathrm{W\cdot m^{-1}\cdot K^{-1}}\right)$	$c\left(\mathrm{J\cdot kg^{-1}\cdot K^{-1}}\right)$	$\rho\left(\mathrm{kg/m^3}\right)$
Panel	8	94.2	1750
Insulation I	0.05	1400	440
Insulation II	0.04	1200	330

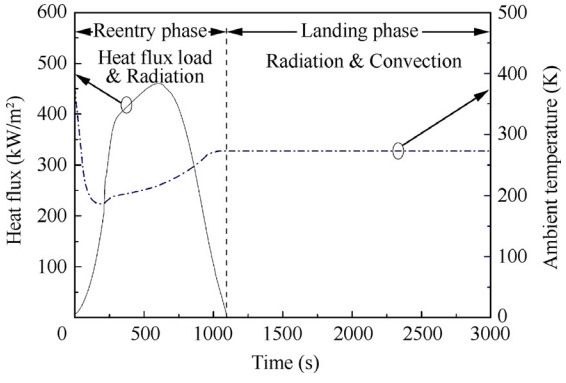

Fig. 11 Heat flux load and ambient temperature.

5.2. Construction of RSA

Form Fig. 13, it can be seen that the finite element analysis needs to continue for long time to obtain the maximum temperature of inner surface, which leads to high computational cost. The quadratic response surfaces of finite element model are built to express the relationships between input variables (including design variables and random parameters) and target responses, as a way to reduce the computation cost in the optimization process. Since we focus on the maximum temperature of TPS during the entire trajectory rather than the local temperature at a fixed point, the response surfaces of the maximum temperatures of TPS's FE model are constructed to approximate the relations between the input parameters and temperature constraints. DOE method is used to generate sampling points for RSA construction. By considering the uncertainties in material properties, the following eight parameters (listed in Table 2) are defined as random variables. The design

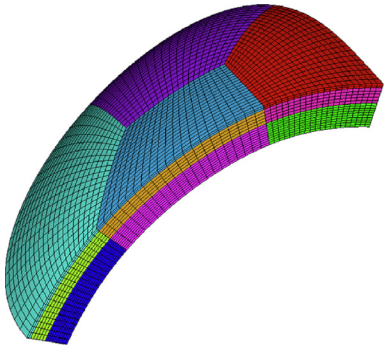

Fig. 12 Finite element model of the nose cone.

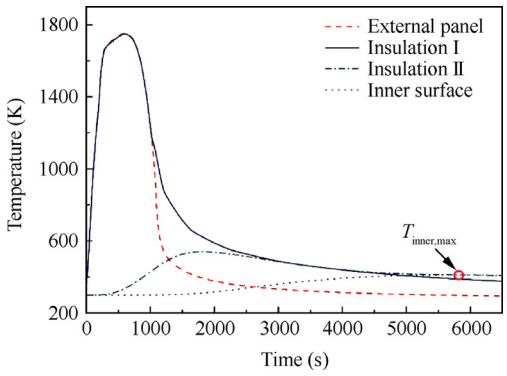

Fig. 13 Temperature profiles of the maximum temperatures of external panel, insulation layers and inner surface.

variables h_1, h_2 are also selected as random variables with coefficient of variation of 0.02.

The sampling data set for DOE will be created by OLH with variations of 6σ around the random variables and the design space of design variables are given in Table 3.

The total number of input parameters is 8 and the quadratic (second order) response surfaces are used in this paper. Accordingly, the minimum number of sampling points is $(8+1)(8+2)/2 = 45$. Therefore, a sampling data set of 45 points is used to generate the first response surfaces. The predicted values of 20 error analysis sampling points are compared with the actual values obtained by finite element analysis, as depicted in Fig. 14. The error estimates of the response surfaces are given in Table 4 to illustrate the accuracy of RSA. From Fig. 14 and Table 4, we can see that the predicted values accord with the actual values across the entire design space.

In engineering practice, the uncertainty of composite material properties will increase, which may be much greater than 0.02. The increase in the uncertainty of material properties will lead to larger design space for DOE to construct the response surface. To solve the problems with large uncertainty level, more sampling points should be generated or some other DOE methods such as central composite design[47] and improved LHS[48] could be employed to obtain desirable response surface approximation.

5.3. Deterministic optimization

The TPS is first optimized deterministically to identify a feasible design from which to begin six sigma robust optimization for quality measurement and improvement. The TPS is to be designed for minimum weight subject to constraints on the maximum temperatures of each insulation layer and inner surface. The values of the uncertainties are set to be the mean values. To find the optimal thicknesses of the insulation layers, the ranges of the thicknesses are assumed as

$$h_1 = 10 \quad \text{to} \quad 30\,\text{mm}$$
$$h_2 = 20 \quad \text{to} \quad 40\,\text{mm}$$

The temperature limits of the insulation layers and inner surface are 1800 K, 720 K, 473 K, respectively. The RSAs constructed in Section 5.2 are used to evaluate the objective function and constraints during the optimization process.

This study uses the NLPQL method to obtain the optimal solution. The parametric modeling is carried out by CATIA and thermal analysis is conducted by ANSYS. The integration of these two modules is achieved by iSIGHT. The optimal solution is listed in Table 5 and the actual values of objective function and constraints at the optimal point obtained by Finite Element Method (FEM) are also given. We can see that there are large deviation between the values of constraints obtained by RSA and FEM, especially for $T_{\text{inner,max}}$. Therefore, the response surfaces constructed in Section 5.2 will be updated by SRSM to improve their accuracies around the optimal point. The optimization history using SRSM is given in Table 6. For each iteration, $n = 8$ (the number of input variables) sampling points generated from subregion are added into the previous sampling data set to reconstruct a new RSA. As seen in Table 6, the optimal solution converges after 5 iterations with optimum values of $h_1 = 15.301$ mm and $h_2 = 27.136$ mm, resulting in a weight reduction of 13.5%.

However, this design has two active constraints: the maximum temperatures of the second insulation layer and inner surface. To analyze the quality of the deterministic design, the six sigma analysis is performed at the optimal solution with consideration of the uncertainties existing in material parameters (see Table 2) and design variables h_1, h_2. By means of RSA, the six sigma analysis will be implemented by Monte Carlo method. The quality results are given in Table 7 alongside the deterministic optimization solution, in which Rel. denotes Reliability.

Table 3 Design space of design variables for DOE.

Bound	Lower bound	Upper bound
h_1 (mm)	10	30
h_2 (mm)	20	40

Table 2 Random variables in material properties.

Parameter	Distribution	Mean	Coefficient of variation	Standard deviation
$k_1(\text{W/m}\cdot\text{K})$	Normal	0.05	0.02	1.0×10^{-3}
$k_2(\text{W/m}\cdot\text{K})$	Normal	0.04	0.02	0.8×10^{-3}
$\rho_1(\text{kg/m}^3)$	Normal	440	0.02	8.8
$\rho_2(\text{kg/m}^3)$	Normal	330	0.02	6.6
$c_1(\text{J}\cdot\text{kg}^{-1}\cdot\text{K}^{-1})$	Normal	1400	0.02	28
$c_2(\text{J}\cdot\text{kg}^{-1}\cdot\text{K}^{-1})$	Normal	1200	0.02	24

Where subscripts 1, 2 denote the first insulation layer and second insulation layer, respectively.

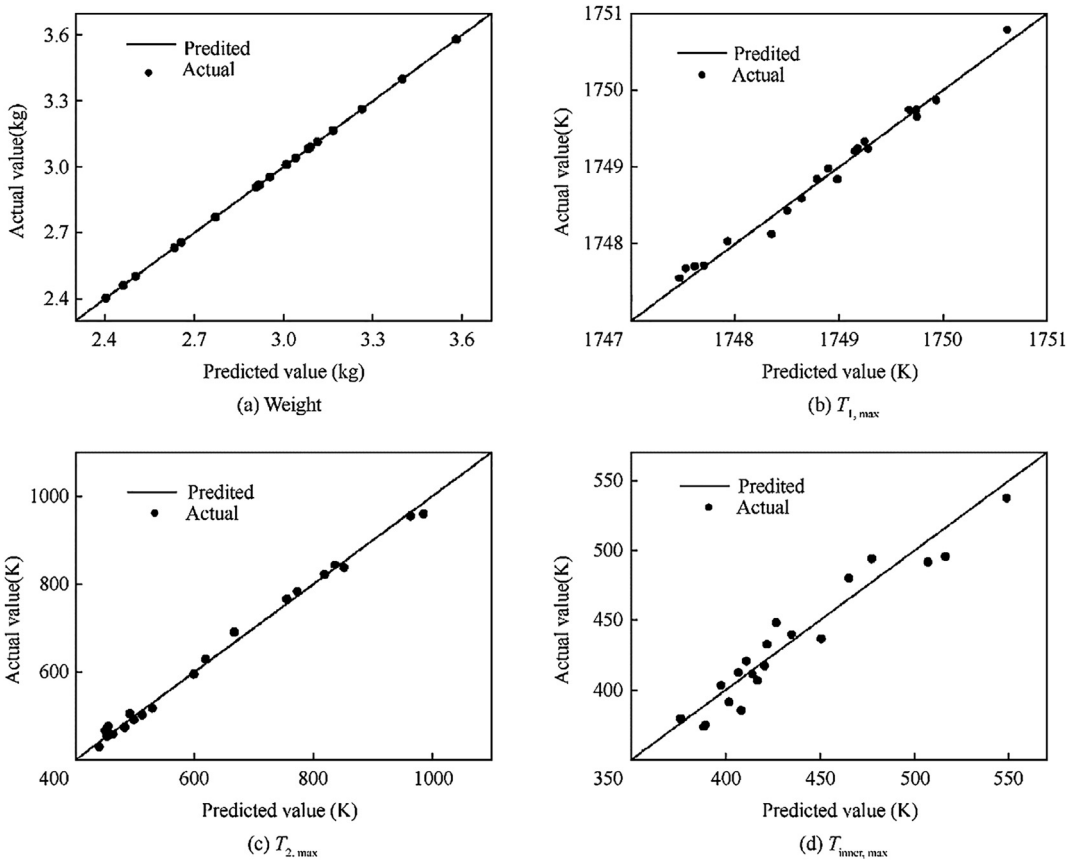

Fig. 14 Comparison between predicted values and actual values.

Table 4 Error values of RSAs (Root mean square).

Parameter	Weight	$T_{1,\max}$	$T_{2,\max}$	$T_{\text{inner},\max}$
Error	2.1129×10^{-4}	0.03217	0.02333	0.07602

As Table 7 indicates, the quality of deterministic design has 0.686σ level and reliability of 50.70% for $T_{2,\max}$, and 0.643σ level and reliability of 48.01% for $T_{\text{inner},\max}$. The probability distributions of active constraints are displayed pictorially in Fig. 15. From Fig. 15, the overall quality or sigma level is different from the sigma position of the upper bound. For example, with a single upper bound at 0.017σ as shown in Fig. 15(a), the percent of the distribution variation outside the constraint is equivalent to that with symmetric lower and upper bounds at $\pm 0.686\sigma$ around the mean, and thus the overall quality level is 0.686σ. It can be observed that almost entire right half of the

Table 5 Optimization results obtained by RSA and FEM.

Solution	h_1 (mm)	h_2 (mm)	W (kg)	$T_{1,\max}$ (K)	$T_{2,\max}$ (K)	$T_{\text{inner},\max}$ (K)
RSA	15.366	32.524	2.847	1748.60	720.00	473.00
FEM			2.848	1748.77	712.10	440.74

Table 6 The deterministic optimization history based on SRSM.

Iteration number	h_1 (mm)	h_2 (mm)	W (kg)	$T_{1,\max}$ (K)	$T_{2,\max}$ (K)	$T_{\text{inner},\max}$ (K)
Baseline	22.000	32.000	3.098	1748.98	540.85	411.72
1	15.366	32.524	2.847	1748.60	720.00	473.00
2	15.877	28.786	2.755	1748.80	720.00	464.04
3	15.362	27.313	2.688	1748.80	720.00	473.00
4	15.396	27.096	2.682	1748.80	719.87	473.00
5	15.301	27.136	2.680	1748.80	720.00	473.00

Table 7 Quality analysis results of deterministic optimization solution.

	Baseline	Deterministic optimization		Six sigma analysis	
Temperature		μ	σ	Rel. (%)	Sigma level
$T_{1,\max}$(K)	1748.98	1748.80	0.169	100	>8.0
$T_{2,\max}$(K)	540.85	719.67	18.705	50.70	0.686
$T_{\text{inner,max}}$(K)	411.72	473.36	7.211	48.01	0.643

Rel. denotes reliability.

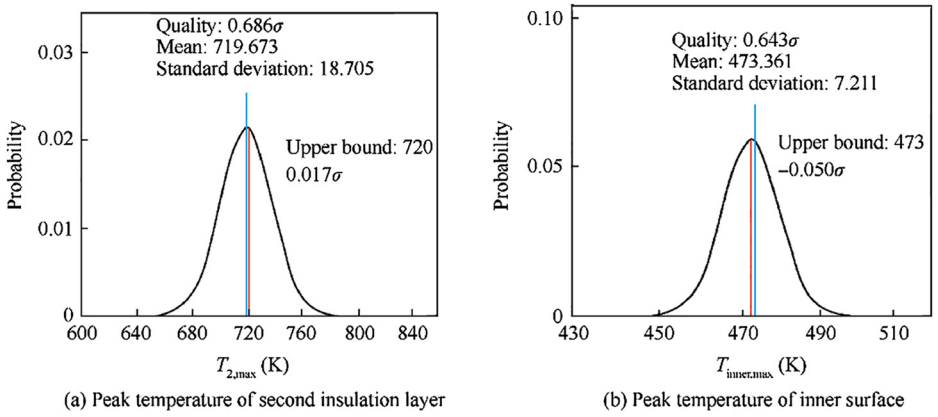

Fig. 15 Constraints quality for deterministic optimization solution.

distribution exceeds the constraint boundary. Obviously, the reliabilities of the active constraints are less than desirable values.

5.4. Reliability-based optimization

In the previous step, the probability of success is estimated to be around 50% for deterministic optimization. To improve the reliability associated with these active constraints, reliability-based optimization is implemented by converting the constraints to probabilistic constraints as follows:

$$\begin{cases} \text{find} & \boldsymbol{d} \\ \text{min} & \mu_{\text{W}} \\ \text{s.t.} & P\left(T_{1,\max} \le T_1^{\text{limit}}\right) \ge \beta_1 \\ & P\left(T_{2,\max} \le T_2^{\text{limit}}\right) \ge \beta_2 \\ & P\left(T_{\text{inner,max}} \le T_{\text{inner}}^{\text{limit}}\right) \ge \beta_3 \\ & \boldsymbol{d}^{\text{L}} \le \boldsymbol{d} \le \boldsymbol{d}^{\text{U}} \end{cases} \tag{14}$$

where $P\left(T_{1,\max} \le T_1^{\text{limit}}\right)$, $P\left(T_{2,\max} \le T_2^{\text{limit}}\right)$, and $P\left(T_{\text{inner,max}} \le T_{\text{inner}}^{\text{limit}}\right)$ denote the reliability indices of $T_{1,\max}$, $T_{2,\max}$, and $T_{\text{inner,max}}$, respectively; β_1, β_2, and β_3 are the reliability criteria for $T_{1,\max}$, $T_{2,\max}$, and $T_{\text{inner,max}}$, respectively. The reliability criteria are set as 99.9999998%, which is equivalent to the design for a quality level of 6 sigma with respect to design specification limits. The optimization history is given in Table 8. From Table 8, the 99.9999998% reliability goal is achieved or exceeded for all constraints. The two active constraints in the deterministic optimization are no longer active even for the specified target reliability.

5.5. Six sigma robust optimization

In this subsection, the six sigma robust optimization is implemented based on response surface in this subsection. Similarly, the RSAs of objective and constraints need to be updated around the design point to acquire a higher accuracy by the method established in Section 5.2. The history of six sigma robust optimization based on SRSM is given in Table 9.

Table 8 Reliability-based optimization history based on SRSM.

Iteration number	h_1(mm)	h_2(mm)	W (kg)		$T_{1,\max}$ (K)		$T_{2,\max}$ (K)		$T_{\text{inner,max}}$ (K)	
			μ	σ	μ	Rel. (%)	μ	Rel. (%)	μ	Rel. (%)
Initial	15.301	27.136	2.680	0.0262	1748.8	100	719.67	50.70	473.36	48.01
1	20.524	27.186	2.898	0.0268	1748.9	100	560.66	100	437.09	100
2	21.104	25.574	2.871	0.0266	1748.9	100	546.30	100	442.10	100
3	20.861	25.402	2.856	0.0265	1748.9	100	554.93	100	443.89	100
4	20.819	25.408	2.854	0.0265	1748.9	100	554.13	100	444.45	100

Table 9 History of six sigma robust optimization based on SRSM.

Iteration number	h_1 (mm)	h_2 (mm)	W (kg)		$T_{1,\max}$ (K)		$T_{2,\max}$ (K)		$T_{\text{inner,max}}$ (K)	
			μ	σ	μ	σ level	μ	σ level	μ	σ level
Initial	15.301	27.136	2.680	0.0262	1748.8	> 8.0	719.67	0.686	473.36	0.643
1	18.357	30.054	2.895	0.0263	1748.8	> 8.0	620.57	6.01	435.46	6.0
2	18.076	29.885	2.878	0.0263	1748.8	> 8.0	628.85	6.0	439.33	6.0
3	18.024	29.881	2.870	0.0263	1748.8	> 8.0	628.58	6.0	439.32	6.0
4	18.071	29.512	2.868	0.0263	1748.8	> 8.0	627.15	6.0	441.05	6.1

Table 10 Comparison between deterministic optimization, reliability-based optimization and six sigma robust optimization.

Parameter	Baseline	DO		RBO		SSRO	
		Solution	Quality	Solution	Quality	Solution	Quality
h_1 (mm)	22.00	15.301		20.819		18.071	
h_2 (mm)	32.00	27.136		25.408		29.512	
W (kg)	3.098	μ 2.680		2.854		2.868	
		σ 0.0262		0.0265		0.0263	
$T_{1,\max}$ (K)	1748.98	μ 1748.8	> 8.0 σ	1748.9	100% Rel.	1748.8	> 8.0 σ
		σ 0.169	(100% Rel.)	0.170		0.167	(100% Rel.)
$T_{2,\max}$ (K)	540.85	μ 719.67	0.686σ	554.13	100% Rel.	627.15	6.0 σ
		σ 18.705	(50.70% Rel.)	17.417		15.471	(~100% Rel.)
$T_{\text{inner,max}}$ (K)	411.72	μ 473.36	0.643 σ	444.45	100% Rel.	441.05	6.1 σ
		σ 7.211	(48.01% Rel.)	6.577		5.796	(~100% Rel.)

The comparison between the Deterministic Optimization (DO), Reliability-Based Optimization (RBO) and Six Sigma Robust Optimization (SSRO) is given in Table 10. From Table 10, compared with deterministic optimization, the quality level is increased for two active constraints by six sigma robust optimization. The sigma level is improved from 0.686σ to 6σ for the maximum temperature of second insulation layer and from 0.643σ to 6.1σ for the maximum temperature of inner surface. It means that the reliability is nearly 100%. For the reliability-based optimization, the mean value of the weight is $\mu_W = 2.854$ and the standard deviation is $\sigma_W = 0.0265$. By means of six sigma robust optimization, the mean value of weight is 2.868 and the standard deviation is 0.0263, which is smaller than that from reliability-based optimization. Similarly, the variations of the temperature constraints, i.e. $\sigma_{T_{1,\max}}, \sigma_{T_{2,\max}}$, and $\sigma_{T_{\text{inner,max}}}$, are also reduced by the six sigma robust optimization. Therefore, it can be concluded that the variations of objective and constraints due to uncertain parameters obtained by six sigma robust optimization are smaller than those obtained by reliability-based optimization, indicating that the former design is more robust. Based on the above discussions, compared with deterministic optimization and reliability-based optimization, the design quality including reliability and robustness is improved by six sigma robust optimization. Meanwhile, the trade-off of increasing the quality is an increase in weight. The weight is increased over the deterministic optimal solution, but is still less than the baseline design.

6. Conclusions

In this paper, a SRSM based six sigma robust optimization approach for the TPS of hypersonic vehicles is proposed to achieve the reduction of structural weight and improvement of design reliability and robustness considering the uncertainties in material properties and geometry. The transient heat transfer analysis for TPS is modeled along the data points selected from the entire trajectory to capture the peak temperatures of the insulation layers and inner surface of TPS. Based on the thermal analysis, the deterministic optimization model is established with the total weight of TPS as objective function and the temperature limitations of insulation layers and inner surface as constraints, to find the optimal thicknesses of insulation layers. By converting the objective to minimizing both the variation and mean performance, and reformulating the constraints as sigma level quality constraints, a six sigma robust optimization for the TPS is presented. In order to reduce computation cost, the quadratic RSM is employed to approximate the values of objective function and constraints. The SRSM based optimization combining response surface updating and optimization strategy is proposed to obtain the true optimal solution. The proposed optimization method is demonstrated in this paper for a nose cone of hypersonic vehicle cabin. The results show that, by using successive response surface in optimization process, the computation cost is reduced and the accuracy of RSA is improved. Compared with deterministic optimization and reliability-based optimization, the six sigma robust optimization notably improves the reliability and robustness of the design, which will have important guiding significance for the optimization design and safety of the TPS in practical engineering.

Acknowledgments

The paper was supported by the National Key Research and Development Program of China (No. 2016YFB0200700), the National Nature Science Foundation of China (No. 11872089, No. 11572024, No. 11432002), and Defence

Industrial Technology Development Programs of China (No. JCKY2016601B001, No. JCKY2016204B101, No. JCKY2017601B001) for the financial supports.

References

1. Gori F, Corasaniti S, Worek WM, Minkowycz WJ. Theoretical prediction of thermal conductivity for thermal protection systems. *Appl Therm Eng* 2012;**49**:124–30.
2. Ma Y, Xu B, Chen M, He R, Wen W, Cheng T. Optimization design of built-up thermal protection system based on validation of corrugated core homogenization. *Appl Therm Eng* 2017;**115**:491–500.
3. Huang C, Yue Z. Calculation of high-temperature insulation parameters and heat transfer behaviors of multilayer insulation by inverse problems method. *Chin J Aeronaut* 2014;**27**(4):791–6.
4. Sun J, Zhang G, Vlahopoulos N, Hong SB. Multi-Disciplinary design optimization under uncertainty for thermal protection system applications. *11th AIAA/ISSMO multidisciplinary analysis and optimization conference*; 2006 Sep 6–8; Virginia, USA. Reston: AIAA; 2006. p. 1–14.
5. Zhao S, Li J, Zhang C, Zhang W, Lin X, He X. Thermo-structural optimization of integrated thermal protection panels with one-layer and two-layer corrugated cores based on simulated annealing algorithm. *Struct Multidiscip Optim* 2014;**51**(2):479–94.
6. Yan W, Luo X, Cui D. Strength Analysis and optimization technique for thermal protection system using 3 dimensional element model. *AIAA modeling and simulation technologies conference*; 2015 Jun 22–26; Dallas, TX, USA. Reston: AIAA; 2015. p. 1–9.
7. Garcia F, Fowler WT. Thermal protection system weight minimization for the space shuttle through trajectory optimization. *J Spacecraft Rockets* 1974;**11**(4):241–5.
8. Shi S, Dai C, Wang Y. Design and optimization of an integrated thermal protection system for space vehicles. *20th AIAA international space planes and hypersonic systems and technologies conference*; 2015 Jul 6–9; Glasgow, Scotland, UK. Reston: AIAA; 2015. p. 1–18.
9. Xie G, Wang Q, Sunden B, Zhang W. Thermomechanical optimization of lightweight thermal protection system under aerodynamic heating. *Appl Thermal Eng* 2013;**59**(1–2):425–34.
10. Deng Z, Guo Z, Zhang X. Non-probabilistic set-theoretic models for transient heat conduction of thermal protection systems with uncertain parameters. *Appl Thermal Eng* 2016;**95**:10–7.
11. Kumar S, Mahulikar SP. Design of thermal protection system for reusable hypersonic vehicle using inverse approach. *J Spacecraft Rockets* 2017;**54**:436–46.
12. Wright MJ, Bose D, Chen YK. Probabilistic modeling of aerothermal and thermal protection material response uncertainties. *AIAA J* 2007;**45**(2):399–410.
13. Ravishankar B, Haftka R, Sankar B. Uncertainty analysis of integrated thermal protection system with rigid insulation bars. *52nd AIAA/ASME/ASCE/AHS/ASC structures, structural dynamics and materials conference*; 2011 Apr 4–7; Denver, Colorado, USA. Reston: AIAA; 2011. p. 1–17.
14. Lv Z, Qiu Z. An iteration method for predicting static response of nonlinear structural systems with non-deterministic parameters. *Appl Math Model* 2018;**68**:48–65.
15. Wang L, Xiong C, Wang XJ, Xu MH, Li YL. A dimension-wise method and its improvement for multidisciplinary interval uncertainty analysis. *Appl Math Model* 2018;**59**:680–95.
16. Lv Z, Liu H. Uncertainty modeling for vibration and buckling behaviors of functionally graded nanobeams in thermal environment. *Compos Struct* 2018;**184**:1165–76.
17. Wang L, Liang JX, Wu D. A non-probabilistic reliability-based topology optimization (NRBTO) method of continuum structures with convex uncertainties. *Struct Multidiscip Optim* 2018;**58**:2601–20.
18. Raisrohani M, Xie Q. Probabilistic structural optimization under reliability, manufacturability, and cost constraints. *AIAA J* 2015;**43**(4):864–73.
19. Qiu Z, Yang D, Elishakoff I. Probabilistic interval reliability of structural systems. *Int J Solids Struct* 2008;**45**(10):2850–60.
20. Byrne DM, Taguchi S. The Taguchi approach to parameter design. *Quality Progress* 1987;**20**(12):19–26.
21. Gunawan S, Azarm S. Multi-objective robust optimization using a sensitivity region concept. *Struct Multidiscip Optim* 2004;**29**(1):50–60.
22. Kolodziej P, Rasky D. Estimates of the orbiter RSI thermal protection system thermal reliability. *36th AIAA thermophysics conference*; 2003 Jun 23–26; Orlando, Florida, USA. Reston: AIAA; 2003. p. 1–20.
23. Kumar S, Villanueva D, Sankar BV, Haftka RT. Probabilistic optimization of integrated thermal protection system. *12th AIAA/ISSMO multidisciplinary analysis and optimization conference*; 2008 Sep 10–12; Victoria, British Columbia, Canada. Reston: AIAA; 2008. p. 1–12.
24. Mazzaracchio A, Marchetti M. A probabilistic sizing tool and Monte Carlo analysis for entry vehicle ablative thermal protection systems. *Acta Astronaut* 2010;**66**(5–6):821–35.
25. Koji S, Akira O, Kozo F. Multi-objective six sigma approach applied to robust airfoil design for mars airplane. *48th AIAA/ASME/ASCE/AHS/ASC structures, structural dynamics, and materials conference*; 2007 Apr 23–26; Honolulu, Hawaii, USA. Reston: AIAA; 2007. p. 1–10.
26. Vlahinos A, Kelkar SG. Designing for six-sigma quality with robust optimization using CAE. *International body engineering conference & exhibition and automotive & transportation technology conference*; 2002 Jul 9–11; Paris, France. Reston: AIAA; 2002. p. 1–8.
27. Smith CF. Six sigma methods applied to an inlet particle separator design. *13th AIAA/ISSMO multidisciplinary analysis optimization conference*; 2010 Sep 13–15; Fort Worth, Texas, USA. Reston: AIAA; 2010. p. 1–10.
28. Schroeder RG, Linderman K, Liedtke C, Choo AS. Six sigma: definition and underlying theory. *J Oper Manage* 2008;**26**(4):536–54.
29. Koch PN, Yang RJ, Gu L. Design for six sigma through robust optimization. *Struct Multidiscip Optim* 2004;**26**(3–4):235–48.
30. Shimoyama K, Oyama A, Fujii K. Development of multi-objective six sigma approach for robust design optimization. *J Aerospace Comput Inf Commun* 2008;**5**:215–33.
31. Asafuddoula M, Singh HK, Ray T. Six-sigma robust design optimization using a many-objective decomposition-based evolutionary algorithm. *IEEE Trans Evol Comput* 2015;**19**(4):490–507.
32. Martin JD, Simpson TW. Use of Kriging models to approximate deterministic computer models. *AIAA J* 2005;**43**(4):853–63.
33. Franklin J. The elements of statistical learning: data mining, inference and prediction. *J Am Stat Assoc* 2010;**173**(3):693–4.
34. Gunst RF. Response surface methodology: process and product optimization using designed experiments. *J Statistical Plann Inference* 1997;**59**(1):185–6.
35. Bai YC, Han X, Jiang C, Bi RG. A response-surface-based structural reliability analysis method by using non-probability convex model. *Appl Math Model* 2014;**38**(15–16):3834–47.
36. Ying WL, Fred M. A sequential response surface method and its application in the reliability analysis of aircraft structural systems. *Struct Safety* 1994;**16**:39–46.
37. Roux WJ, Stander N, Haftka RT. Response surface approximations for structural optimization. *Int J Numer Meth Eng* 2015;**42**(3):517–34.
38. Johnson T, Waters W, Singer T, Haftka R. Thermal-structural optimization of integrated cryogenic propellant tank concepts for a reusable launch vehicle. *45th AIAA/ASME/ASCE/AHS/ASC structures, structural dynamics and materials conference*; 2004 Apr 893 19–22; Palm Springs, California, USA. Reston: AIAA. p. 1–11.

39. Kurtaran H, Eskandarian A, Marzougui D, Bedewi NE. Crashworthiness design optimization using successive response surface approximations. *Comput Mech* 2002;**29**(4–5):409–21.
40. Kim SH, Na SW. Response surface method using vector projected sampling points. *Struct Saf* 1997;**19**(1):3–19.
41. Giunta AA, Balabanov V, Haim D, Bernard G, Mason WH, Waston LT. Multidisciplinary optimization of a supersonic transport using design of experiments theory and response surface modelling. *Aeronaut J* 1997;**101**(1008):347–56.
42. Wang GG. Adaptive response surface method using inherited latin hypercube design points. *J Mech Des* 2003;**125**(2):210–20.
43. Xie GN, Qi W, Zhang WH, Sunden B, Lorenzini G. Optimization design and analysis of multilayer lightweight thermal protection structures under aerodynamic heating conditions. *J Therm Sci Eng Appl* 2013;**5**(1) 011011.
44. Poteet CC, Abu-Khajeel H, Hsu SY. Preliminary thermal-mechanical sizing of a metallic thermal protection system. *J Spacecraft Rockets* 2004;**41**(2):173–82.
45. Shimoyama K, Oyama A, Fujii K. A new efficient and useful robust optimization approach design for multi-objective six sigma. *Proceedings of the 2005 IEEE congress on evolutionary computation*; 2005 Sep 2-4; Edinburgh, UK.Piscataway(NJ): IEEE Press; 2005. p. 950-957.
46. Devanathan S, Koch PN. Comparison of meta-modeling approaches for optimization. *Proceedings of the ASME 2011 international mechanical engineering congress and exposition*; 2011 Nov 11–17; Denver, Colorado, USA. New York: ASME; 2011. p. 1–9.
47. Montazer M, Taghavi FA, Toliyat T, Moghadam MB. Optimization of dyeing of wool with madder and liposomes by central composite design. *J Appl Polym Sci* 2010;**106**(3):1614–21.
48. Yu H, Chung CY, Wong KP, Lee HW, Zhang JH. Probabilistic load flow evaluation with hybrid Latin hypercube sampling and cholesky decomposition. *IEEE Trans Power Syst* 2009;**24**(2):661–7.